

Bundle Networks: Fiber Bundles, Local Trivializations, and a Generative Approach to Exploring Many-to-one Maps

Nico Courts *

Department of Mathematics

University of Washington

Seattle, WA

`ncourts@math.washington.edu`

Henry Kvinge

Pacific Northwest National Laboratory

Seattle, WA

`henry.kvinge@pnnl.gov`

Abstract

Many-to-one maps are ubiquitous in machine learning, from the image recognition model that assigns a multitude of distinct images to the concept of “cat” to the time series forecasting model which assigns a range of distinct time-series to a single scalar regression value. While the primary use of such models is naturally to associate correct output to each input, in many problems it is also useful to be able to explore, understand, and sample from a model’s fibers, which are the set of input values x such that $f(x) = y$, for fixed y in the output space. In this paper we show that popular generative architectures are ill-suited to such tasks. Motivated by this we introduce a novel generative architecture, a Bundle Network, based on the concept of a fiber bundle from (differential) topology. BundleNets exploit the idea of a local trivialization wherein a space can be locally decomposed into a product space that cleanly encodes the many-to-one nature of the map. By enforcing this decomposition in BundleNets and by utilizing state-of-the-art invertible components, investigating a network’s fibers becomes natural.

1 Introduction

In the last decade, generative methods have made remarkable strides toward the goal of faithfully modeling complex data distributions. Families of model architectures such as generative adversarial networks (GANs) [GPAM⁺14], variational autoencoders (VAEs) [KW13], and normalizing flows [RM15] have enabled a range of tasks that were previously thought to be unachievable for complex (and often high-dimensional) distributions such as those representing natural images. Applications include image to image translation [MLT⁺19, LTH⁺18], music generation [Mog16], image super-resolution [LTH⁺17], and density estimation [DSB16]. In this work we introduce a new task in machine learning which revolves around the problem of modeling the structure of many-to-one maps.

The majority of classification and regression tasks in machine learning involve many-to-one maps. That is, maps that send a range of distinct inputs to the same output. For example, most image recognition tasks are many-to-one since they send an infinite set of natural images to a finite number of classes. Of course, there is no reason that a model’s target space needs to be discrete—consider, for instance, a sentiment analysis task where sentiment is naturally represented by a continuum. There are likely a range of distinct

*Work completed during an internship at Pacific Northwest National Laboratory.

expressions that result in the same sentiment value. While the focus of most research on such tasks is training models that give correct predictions, it can also be useful to be able to fix an output value y and explore, quantify, or sample from all those x which map to y . Such an exercise allows one to understand different modes of variation that a classification or regression model collapses in the process of making its predictions. If function $\pi : X \rightarrow Y$ is the ground truth pairing between input space X and output space Y , this amounts to calculating the inverse image $\pi^{-1}(y)$, or *fiber* of π at y .

Our goal in the present work is to (1) formalize this problem and (2) describe a deep learning framework which readily enables this kind of analysis. We take as our inspiration the notion of a fiber bundle from topology [Sei33, Whi35]. Consider the projection map on $X = Y \times Z$, $\pi : Y \times Z \rightarrow Y$, which sends $\pi(y, z) = y$. For any $y \in Y$, the inverse image $\pi^{-1}(y)$ is easily calculated as $\{y\} \times Z \cong Z$. Interpreted in terms of the machine learning task, Y is the component of X that we want to predict and Z encodes the remaining variation occurring among all x that map to y . Unfortunately, in our nonlinear world data distributions can rarely be decomposed into a product space on a global level like this. Instead, it is more realistic to hope that for each sufficiently small neighborhood U of Y , we can find a data distribution preserving homeomorphism $U \times Z \xrightarrow{\sim} \pi^{-1}(U)$. This informally summarizes the idea of a fiber bundle, where locally the space X is the product of a base space (some subset of Y) and a fiber Z . Following the mathematical literature, we call this task *local trivialization of X* . A local trivialization is useful since it allows us to understand and explore the fibers of π .

In our experiments we show that popular generative models including Wasserstein GANs [WHT⁺18] and conditional GANs [MO14], are unable to accurately model the fiber structure of a machine learning task. To address this, we describe a new deep learning architecture called a *Bundle Network* which is designed to produce local trivializations of an input space X and thus enable one to model fibers of a task. Bundle Networks use clustering algorithms to divide up the output space Y into neighborhoods $\{U_i\}$ and then learn a conditioned, invertible mapping that decomposes the inverse image of each of these neighborhoods $\pi^{-1}(U_i)$ into a product $U_i \times Z$ that preserves the distributions induced by the data.

We show that Bundle Networks can effectively model fibers for a range of datasets and tasks, from synthetic datasets that represent classic examples of fiber bundles, to the Wine Quality [CCA⁺09] and Airfoil Noise [BPM89] datasets from [DG17]. In the former of these Y is a discrete space, while in the latter Y is continuous. We end the paper by discussing the choice of fiber space Z that must be made when initializing a Bundle Network. We show that if one makes sound topological choices for Z , Z is robust to differences in fiber structure within a single task.

In summary, our contributions in this paper include the following.

- We identify and formalize the problem of *learning the fibers* of a machine learning task.
- We describe one approach to solving this problem, using a fiber bundle framework to learn how to locally decompose the input space of the task into a product of label space and a fiber space that parametrizes all additional variation in the data.
- We introduce a new family of deep generative models called a Bundle Network and show via empirical experiments that, while other popular architectures struggle to model the fibers of a machine learning task, Bundle Networks yield strong results.

2 Related work

There are a range of topics in generative deep learning that are related to the task and model that we introduce in this paper. Below we highlight some of the most important.

Conditional generative models: The local trivialization task that we describe in Section 3.1 can be interpreted as a special type of conditional generative task. That is, a task where data generation is conditioned on some additional variables. Common models within this framework are the various flavors of conditional variational autoencoders (VAE) [SLY15] and conditional generative adversarial networks (GAN) [MO14]. While our approach utilizes conditional components to capture differences in model behavior at

different locations in input space, additional aspects of the task, such as the local decomposition of input space into fiber and label space, mean that without extra modification, standard generative models do not give strong results. We show this in our experiments in Section 5.

Invertible neural networks: Invertible neural networks have recently become a topic of interest within the deep learning community. Some of the first network layers that were both invertible and learnable were suggested in [DKB15, DSB16] and are in essence affine transformations followed by coordinate permutations (or an orthogonal transformation). The weights and biases used in each affine block, however, are conditioned on the input itself, meaning that stacking multiple invertible blocks can give models with impressive expressive power. [AKRK18] and [SRK20] are among the works that have used invertible networks to solve problems of distribution approximation with the latter introducing general incompressible-flow networks (GINs) which are volume-preserving versions of invertible neural networks. The most common instance of invertible neural networks are normalizing flows, which were popularized by [RM15] and have a number of capabilities not found in the more popular GAN and VAE approaches, such as density estimation.

Feature disentanglement: Distribution disentanglement is (roughly) the task of learning a latent space for a distribution such that orthogonal directions capture independent and uncorrelated modes of variation in the data. There have been a broad range of methods developed to solve the nonlinear version of this problem. Most modify popular generative models such as generative adversarial networks (GANs) and variational autoencoders (VAEs) [CLGD18, KM18, Dup18, CDH⁺16, LTFO20]. Like disentanglement, the local trivialization task described in this paper involves factoring a data distribution. Unlike the problem of feature disentanglement, which generally seeks to decompose a distribution into all independent modes of variation, we only seek to distinguish between those modes of variation defined by the classes or targets of the supervised task and all other variation. The local nature of our factorization further sets us apart from work on feature disentanglement.

3 Fiber bundles and local trivializations

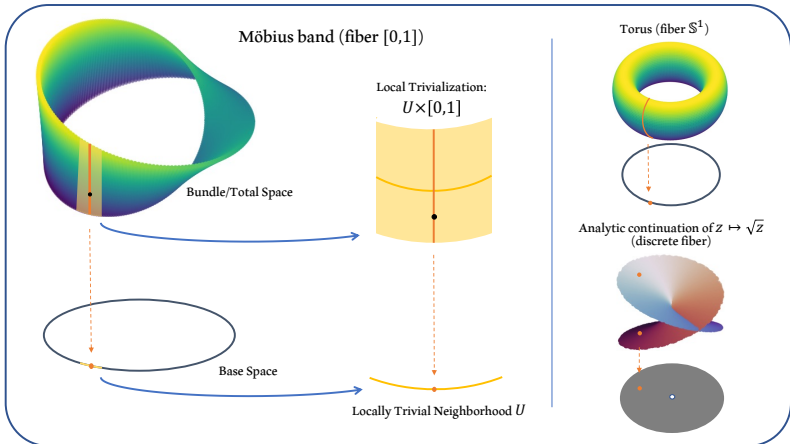


Figure 1: Examples of fiber bundles. **(Left)** A Möbius band as a bundle over the circle S^1 . A typical fiber over a base point (dark orange) and a locally trivial neighborhood and local trivialization are included for illustration. **(Right)** Two other examples of fiber bundles. Above is the Torus (with circular fiber) lying over the circle. Below is the analytic continuation of the complex function $z \mapsto \sqrt{z}$ over the punctured disc $\hat{\mathbb{D}} = \{z \in \mathbb{C} \mid 0 < |z| < 1\}$, which has a two-point fiber.

One way to understand complicated geometric spaces is to decompose them into simpler components. For example, topologically a torus T can be understood to be the product of two circles $T \cong S^1 \times S^1$. Such

decompositions into product spaces are particularly useful in applications since many algorithms on the entire space can then be reduced to independent, component-wise calculations. However, even in situations where local neighborhoods look like a product, such decompositions may not be possible globally because of “twists” that occur in a space (for example in the Möbius band, see Figure 1). First developed in the work of [Sei33] and [Whi35], fiber bundles are a geometric structure designed to capture the **locally** product-like nature of such spaces.

Formally, a *fiber bundle* is a triple (E, B, Z) of topological spaces along with a (surjective) continuous map $\pi : E \rightarrow B$ and a collection of *local trivializations* $\mathcal{T} = \{(U_i, \varphi_i)\}_{i \in \mathcal{I}}$ subject to the conditions that (i) $\{U_i\}_{i \in \mathcal{I}}$ is an open cover of B and (ii) for each $i \in \mathcal{I}$, φ_i gives an homeomorphism $\varphi_i : U_i \times Z \xrightarrow{\cong} \pi^{-1}(U_i)$ such that the obvious projection from $U_i \times Z$ to U_i agrees with the map π restricted from $\pi^{-1}(U_i)$ to U_i . This last condition is equivalent to saying that for all $i \in \mathcal{I}$, the following diagram commutes.

$$\begin{array}{ccc}
 \pi^{-1}(U_i) & \begin{array}{c} \xleftarrow{\varphi_i} \\ \xrightarrow{\varphi_i^{-1}} \end{array} & U_i \times Z \\
 \pi_i \downarrow & \swarrow \text{proj} & \\
 U_i & &
 \end{array} \tag{1}$$

The space E is generally called the *total space*, B is called the *base space*, and Z is called the *fiber*. One can think of this definition as rigorously capturing the idea that for small enough neighborhoods, E looks like the product of a subset of B and Z . Some standard fiber bundles can be found in Figure 1.

3.1 The local trivialization of a machine learning task and modeling data on a fiber

Suppose that \mathcal{T} is a supervised machine learning task that involves taking data from X and predicting a correspond element of Y . Let \mathcal{D}_X be the data distribution on X and let measurable function $\pi : \text{supp}(\mathcal{D}_X) \rightarrow Y$, define a ground truth label for each x in the support of \mathcal{D}_X . Then for any measurable open set $U \subseteq Y$, \mathcal{D}_X induces a conditional distribution, $\mathcal{D}_{\pi^{-1}(U)}$ on $\pi^{-1}(U)$. In a similar fashion, via the pushforward of \mathcal{D}_X using π , we get a label distribution \mathcal{D}_Y on Y . Finally, each measurable subset $U \in Y$ inherits a conditional distribution \mathcal{D}_U from \mathcal{D}_Y . We call the sets $\pi^{-1}(U)$ with distribution $\mathcal{D}_{\pi^{-1}(U)}$ the *trivializable neighborhoods of task \mathcal{T}* .

A *local trivialization* of X with respect to π , involves:

1. A choice of open cover $\mathcal{U} = \{U_i\}$ of Y such that $\cup_i U_i = Y$.
2. A choice of fiber space Z with associated *fiber distribution* \mathcal{D}_Z .
3. Learning an invertible, *trivializing map* $\varphi_i : U_i \times Z \rightarrow \pi^{-1}(U_i)$ for each $U_i \in \mathcal{U}$, such that (a) φ_i maps distribution $\mathcal{D}_{U_i} \otimes \mathcal{D}_Z$ to $\mathcal{D}_{\pi^{-1}(U_i)}$ and (b) φ_i^{-1} makes Diagram 1 commute.

Note that in the above formulation, the space X takes the role of the total space E from section 3 and Y takes the role of the base space B . Though good choices of fiber Z and measure ν can occasionally be guessed based on the nature of the data, they generally must be arrived at through experimentation.

The trivializing maps $\{\varphi_i\}_i$ allow one to explore the fibers of π , which includes sampling from them. For example, if we choose some $y \in Y$ then we can sample from the fiber $\pi^{-1}(y)$ by (1) identifying the neighborhood U_i that y belongs to, (2) sampling a collection of points $\{z_1, \dots, z_\ell\}$ using \mathcal{D}_Z , and (3) applying the map φ_i to (y, z_i) for each $z \in \{z_1, \dots, z_\ell\}$.

4 Bundle Networks

In order to develop a model that can solve the problem described in section 3.1, we introduce the family of *Bundle Networks* (or *BundleNets* for short). A Bundle Network uses invertible components so that φ_i and φ_i^{-1} can both be learned simultaneously. A BundleNet further uses conditioning to avoid needing to

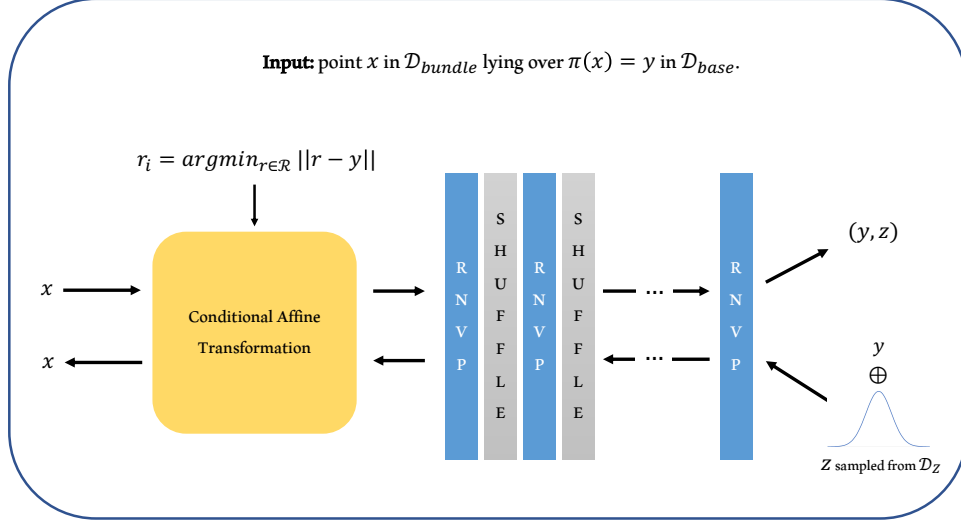


Figure 2: A diagram of the BundleNet architecture. The upper arrows indicate the forward operation of the model while the lower arrows indicate the reverse operation of the model.

train a different model for each U_i in \mathcal{U} . Using the notation from section 3.1, a BundleNet can concretely be understood as a neural network $\Phi : X \times \mathcal{R} \rightarrow Y \times Z$, where \mathcal{R} consists of a set of conditioning vectors so that for any $r \in \mathcal{R}$, $\Phi_i := \Phi(-, r_i) : X \rightarrow Y \times Z$ is an invertible neural network. The elements of \mathcal{R} are in bijection with neighborhoods contained in \mathcal{U} with the objective of having Φ_i play the role of φ_i^{-1} . Moving from forward to back, the first layer of Φ is an affine transformation conditioned (solely) on elements from \mathcal{R} . After this layer, the model consists of alternating RNVP blocks and coordinate permutations.

As noted in section 3.1, a number of choices need to be made before a model is trained. Let $D_t \subseteq X \times Y$ be the training set and $p_X : X \times Y \rightarrow X$ and $p_Y : X \times Y \rightarrow Y$ be the standard projections of $X \times Y$ onto its components. Firstly, the collection of neighborhoods \mathcal{U} in Y needs to be chosen. In the case of regression, where $p_Y(D_t)$ can contain an arbitrary number of distinct elements, we found that using k -means was an efficient and effective way to cluster these points into neighborhoods. The set of cluster centroids are then exactly the vectors $\mathcal{R} = \{r_1, \dots, r_q\}$ that will be used to condition the network. The number of clusters, q , is a hyperparameter that can be explored during training. In the case where the output values are discrete (i.e. $p_Y(D_t)$ can only take a finite number of values $C = \{c_1, \dots, c_q\}$), one can simply set $U_i = \{c_i\}$. After selecting neighborhoods \mathcal{U} in the base space, the neighborhoods in X are defined automatically by taking an inverse image with respect to π . The fiber Z and fiber distribution \mathcal{D}_z also need to be chosen. These choices are discussed in the first part of Section 6.

We call application of the model in the direction $X \rightarrow Y \times Z$ *forward operation* and application of the model in the direction $Y \times Z \rightarrow X$ *reverse operation* in accordance with the ground truth association function $\pi : X \rightarrow Y$. As depicted in Figure 2, to apply Φ to a training point $(x, y) \in D_t$ in the “forward direction” we solve $r_i = \arg \min_{r \in \mathcal{R}} \|r - y\|$, finding the centroid r_i in \mathcal{R} that is closest to label y . Then we apply $\Phi_i = \Phi(-, r_i)$ to x . To run Φ in reverse on training example (x, y) we invert Φ_i to Φ_i^{-1} , sample some z from \mathcal{D}_Z , and compute $\Phi_i^{-1}(y, z)$. To ease notation we write $\Phi(x)$ (respectively, $\Phi^{-1}(y, z)$) to denote process of first computing r_i and then applying Φ_i to x (resp. Φ_i^{-1} to (y, z)).

Since we are primarily interested in generating and sampling from task fibers via their local trivialization, at inference time we only run Φ in reverse, applying Φ_i^{-1} to a collection of points (y, z) sampled from $\mathcal{D}_{U_i} \otimes \mathcal{D}_Z$. We evaluate this mapping by measuring the discrepancy of the resulting image in X against the distribution $\mathcal{D}_{\pi^{-1}(U_i)}$. One could conceivably also use Φ for classification, but in that case one would need to develop a strategy for identifying the proper $r_i \in \mathcal{R}$ to use to condition Φ in the absence of a label associated with

$x \in X$. One could likely use a nearest neighbor approach using points that are known to belong to each $\pi^{-1}(U_i)$, but we leave this for future work.

The loss we choose for our model consists of two main parts, \mathcal{L}_{fwd} and \mathcal{L}_{bwd} , corresponding to loss from the forward and backward directions. Since Φ is invertible, these can be trained simultaneously and updated with a unified gradient step. Together, our final loss is then $\mathcal{L}_{\text{bundlenet}} = \mathcal{L}_{\text{bwd}} + \mathcal{L}_{\text{fwd}}$.

The forward loss \mathcal{L}_{fwd} is the simpler of the pair. Given $(x, y) \in D_t$, we find i such that $y \in U_i$ and compute $\mathcal{L}_{\text{fwd}}(x, y) = \|p_Y(\Phi_i(x)) - y\|^2$, where p_Y denotes the projection from $Y \times Z$ to Y . This term ensures that in the forward direction Φ accurately maps elements from X to base space Y . The backward loss is comprised of several terms: $\mathcal{L}_{\text{bwd}} = \mathcal{L}_{\text{KL-fwd}} + \mathcal{L}_{\text{KL-bwd}} + \mathcal{L}_{\text{MSMD}}$. Choosing some $U_i \in \mathcal{U}$, we sample points from \mathcal{D}_{U_i} and pair each with a point that we sample from our priors (that is, from \mathcal{D}_z) to get a set S . S is passed through Φ_i^{-1} to generate points in X . Then the MSMD, KL-fwd, and KL-bwd losses (cf. section A.2) are used to compute a loss term by comparing $\Phi_i^{-1}(S)$ and points sampled from $\mathcal{D}_{\pi^{-1}(U_i)}$. The KL-divergence terms act to ensure that the two point clouds $\Phi_i^{-1}(S)$ and $\pi^{-1}(U_i)$ cover one another and the MSMD term ensures that no point in $\Phi_i^{-1}(S)$ is too far from some point in $\pi^{-1}(U_i)$.

5 Experiments

We evaluate Bundle Networks on four datasets. Two of them are synthetic and represent classic examples of vector bundles: the Möbius band and the torus, both embedded in \mathbb{R}^3 . The other datasets are Wine Quality [CCA⁺09] and Airfoil Noise [BPM89], both of which are available in the UC Irvine Machine Learning Repository [DG17]. For the invertible layers in BundleNet we used the FrEIA package [AKS⁺21].

We chose Wine Quality and Airfoil Noise because they represented low-dimensional, many-to-one relationships with several continuous variables making each a good first test case for the local trivialization task. We describe the details of these datasets along with our manipulations of them in Appendix section A.1, but the primary difference between the Wine Quality and Airfoil Noise dataset is that the latter has a continuously-valued output (and thus base space) while the former has a discrete number of outputs (13 distinct wine color/quality pairs).

In selecting models against which to compare our BundleNets, we chose modern yet general-purpose models that have proven effective at many generative tasks. This includes Wasserstein divergence GANs (WGAN) developed as an improvement on traditional Wasserstein GANs by [WHT⁺18] and conditional GANs (CGANs) from [MO14]. While WGAN directly learns to approximate the global distribution of data using Wasserstein distance, it doesn't include a conditional aspect that allows a user to specify a fiber to sample from so it is excluded from our fiberwise metrics. We also implement a version of a CGAN we call CGAN-nbhd that conditions on a concatenated vector consisting both of the base point and a neighborhood representative, chosen in a manner analogous to BundleNet. This model was our best effort to equip an existing model from the literature with the same capabilities as BundleNet without in the process creating another novel architecture.

5.1 Training and evaluation procedure

Each model was trained on a single GPU (Nvidia Tesla p100 @ 16GB) for a period of 2000 epochs using an initial learning rate of 10^{-4} which was halved every 70 epochs. The weights that were used for evaluation were the final weights that were saved after the final epoch, even if the model converged long before. A table of hyperparameters used for these results (including fiber distributions \mathcal{D}_Z) can be found in Appendix section A.3.

The aim of our evaluation is to understand how well BundleNet models can reconstruct fibers in the total space X . We use a number of different metrics to do this including: mean squared minimum distance, KL-divergence, Wasserstein metrics, and maximum mean discrepancy. We focus on the Wasserstein-1 metric below (since it is a commonly used tool when measuring the similarity of two distributions) but the full suite of results with all metrics can be found in Appendix section A.5.

Table 1: The Wasserstein-1 metric for global data generation across all four datasets and models. Each metric is applied to a trained model as detailed in section 5.1 with 95% confidence intervals determined by bootstrapping.

	BundleNet (ours)	WGAN	CGAN	CGAN-nbhd
Torus	0.706 ± 0.018	2.192 ± 0.010	7.113 ± 0.024	7.908 ± 0.016
Möbius band	0.264 ± 0.004	2.048 ± 0.013	1.844 ± 0.015	7.764 ± 0.008
Wine Quality	1.733 ± 0.011	99.22 ± 0.392	4.054 ± 0.014	4.405 ± 0.013
Airfoil Noise	1.448 ± 0.022	4.741 ± 0.034	2.508 ± 0.025	4.279 ± 0.019

Table 2: The Wasserstein-1 metric for fiberwise data generation across all four datasets and the three models that have a conditional component. Intervals represent 95% CIs over 10 repeated experiments.

	BundleNet (ours)	CGAN	CGAN-nbhd
Torus	0.743 ± 0.026	7.979 ± 0.022	8.044 ± 0.021
Möbius band	0.279 ± 0.011	9.860 ± 0.038	7.958 ± 0.022
Wine Quality	1.917 ± 0.172	3.666 ± 0.233	4.408 ± 0.457
Airfoil Noise	3.124 ± 0.089	3.563 ± 0.158	3.794 ± 0.128

We perform such measurements in two modes: the *global* and *fiberwise* regimes. In the global regime, the trained model is asked to generate 4000 points from the global distribution D_X (using points sampled from Y and Z) and these are compared against 4000 points from either the true data distribution (in the synthetic datasets when this is known) or from a held-out test set (when we don't have access to the underlying distribution). Then these two point clouds are evaluated using each of our metrics. The process is repeated 10 times and the output values are bootstrapped to compute sample mean with 95% confidence intervals. In the fiberwise regime, 15 points are sampled from Y and for each such y , we use the model to generate 200 points lying in $\pi^{-1}(y)$. We compare this against 200 points we have sampled from either the true fiber (when this is known) or the points lying over the base point in our combined train & test sets. Each metric is evaluated 10 times and bootstrapped as above.

5.2 Results

For the results described in this section we mostly focus on the Wasserstein-1 metric \mathcal{W}_1 as our evaluation statistic. The full suite of results (MSMD, MMD, KL-fwd, KL-bwd, \mathcal{W}_1 , and \mathcal{W}_2) can be found in Appendix section A.5. With a few exceptions, performance patterns we see for the Wasserstein-1 metric are largely repeated when we apply other metrics.

As can be seen in tables 1 and 2, BundleNet outperforms all the other models in terms of the Wasserstein-1 metric, sometimes by a very wide margin, in both the global and fiberwise data generation regimes. In fact, the only statistic for which another model's 95% confidence interval even intersects with BundleNet's is MMD on the Wine Quality and Airfoil Noise datasets, where BundleNet still outperforms its closest competitor CGAN (table 7).

Within the global data generation regime, WGAN comes closest to BundleNet's performance for the synthetic datasets which have more consistent regularity in each fiber, whereas this model's performance plummets on the Wine Quality dataset whose fibers across different wine color/quality pairs differ significantly. We take this as evidence that the problem of learning fibers is best approached locally (as within the fiber bundle or CGAN framework), instead of trying to learn a single global map. In the fiber generation regime, CGAN comes closest to BundleNet's performance on 3 out of the 4 datasets. Consistent with the behavior that was seen in the global regime, the BundleNet's advantage over both variants of CGANs de-

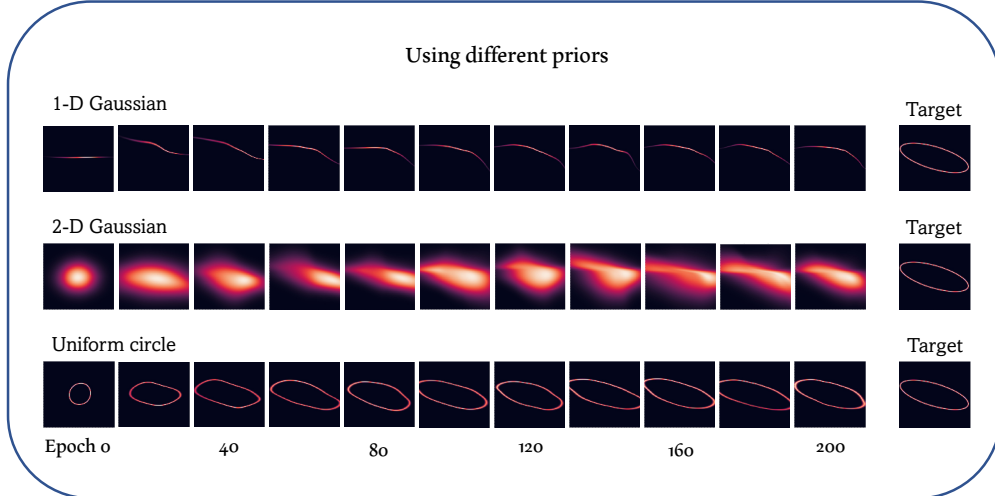


Figure 3: Visualization of the convergence of three different priors to a distribution on an oval (a 1-dimensional Gaussian (**Above**), a 2-dimensional Gaussian (**Middle**), and a uniform distribution on a circle (**Below**)).

creases on the non-synthetic datasets. Further, while conditioning on neighborhood representatives is a core component of BundleNet, we found that including this additional information within the CGAN framework (as CGAN-nbhd does) generally did not result in improved performance. In fact, CGAN beat CGAN-nbhd on 7 out of 8 global and fiberwise tests.

In terms of additional metrics we tested, notable behavior included high variance for the fiberwise MMD metric on the Wine Quality Dataset (this is also one of the two cases where CGANs confidence interval intersected with BundleNet). One reason that this dataset is particularly challenging is that the neighborhoods $\{U_i\}$ are imbalanced: the quality values are much more likely to be in the core 4-6 range. We suspect that learning to model fibers in imbalanced settings will need to be a topic of future research.

6 Discussion

Topological priors on fibers: As mentioned in section 4, BundleNet requires one to choose an underlying fiber distribution \mathcal{D}_Z . The natural choice would be to use Gaussian distributions since they are tractable computationally and to some degree universal in statistics. A natural question is: how well can a Gaussian prior capture more topologically diverse fibers—for example, circular fibers that arise in tasks that involve periodic systems or invariance to 1-dimensional rotations?

To test this, we trained an invertible neural networks to map a 1-dimensional Gaussian, a 2-dimensional Gaussian, and a uniform distribution on a circle to a distribution on an oval in the plane. In each case the model was the same deep invertible architecture with RNVP blocks trained with (forward and backward) KL-divergence. Visualizations of the result can be found in figure 3. As expected the circular distribution quickly converges to the target oval while neither the 1- nor 2-dimensional Gaussian converges to a distribution that is visually similar to the oval. This aligns with the basic fact from topology that there is no continuous bijective map from the interval $[0, 1]$ to the circle S^1 [Lee10]. Based on this observation and the fact that up to homeomorphism the circle and \mathbb{R} are the only two real, connected, 1-dimensional manifolds, we investigated which prior would give better results on our synthetic datasets.

One might expect that the model with Gaussian prior would perform better on the Möbius band, whose fibers are intervals while the circle prior would lead to better performance on the torus whose fibers are

Table 3: The Wasserstein-1 metric for fiberwise data generation for models using either a single 1-dimensional Gaussian or a uniform distribution on the circle as a prior.

	Gaussian prior	Circular prior
Torus (global)	1.640 ± 0.020	1.338 ± 0.005
Möbius band (global)	0.327 ± 0.006	0.240 ± 0.007
Torus (fiberwise)	1.781 ± 0.094	1.312 ± 0.008
Möbius band (fiberwise)	0.411 ± 0.029	0.231 ± 0.016

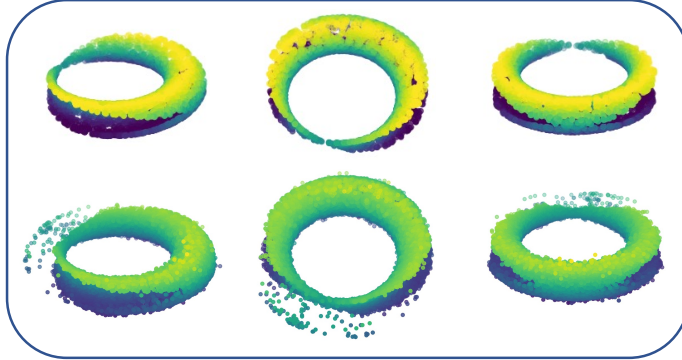


Figure 4: Qualitative ability of BundleNet to generate points on a “bundle” where the fibers have different geometry and topology. **(Above)** The true data distribution we call the sliced torus. **(Below)** 70,000 global points generated by a BundleNet after training.

circles. Surprisingly, the circle prior resulted in the better performance in all settings, torus and Möbius band, fiberwise and globally. A possible explanation for this is that the circle prior is a uniform distribution supported on a compact set. The same is true for the fibers in the Möbius band and it is possible that the model has a harder time concentrating the density of a Gaussian distribution than collapsing the shape of a circle to (approximately) a line segment.

Fiber topology need not be uniform: While the theory of fiber bundles is rich and well-studied in math, it is perhaps restrictive to have to assume that the data that arises in the real world has this very particular and highly-structured form. Our results on the non-synthetic datasets shown in tables 1 and 2, however suggest that the neighborhood-based approach allows BundleNet to be more flexible. To test whether BundleNets can perform well on datasets whose fibers are not all the same (specifically homeomorphic) we train and test it on a new dataset called the *sliced torus* that is identical to our torus dataset except that the fiber varies continuously from a point to a full circle and back as we traverse the ring.

Table 4: Torus vs sliced torus. Torus results are juxtaposed with those of the sliced torus to give an approximate benchmark for comparison since the two point clouds have similar distributions and scale.

	Torus (global)	Sliced (global)	Torus (fiberwise)	Sliced (fiberwise)
MSMD	0.118 ± 0.003	0.052 ± 0.002	0.055 ± 0.004	0.007 ± 0.001
MMD ($\times 10^{-3}$)	0.691 ± 0.025	2.013 ± 0.048	20.89 ± 0.935	11.43 ± 1.040
\mathcal{W}_1	0.706 ± 0.018	1.191 ± 0.024	0.743 ± 0.026	0.207 ± 0.012
\mathcal{W}_2	1.075 ± 0.071	4.560 ± 0.116	0.605 ± 0.035	0.077 ± 0.015

The quantitative results of our experiments can be found in table 4 and qualitative comparisons are made in figure 4. In most cases we see that generative metrics are comparable to those we saw on the torus dataset and almost all cases (except global \mathcal{W}_2) the results on the sliced torus are better than the next best model we tested on the torus dataset. This, coupled with our superior performance on real-world data that is unlikely to take the form of a true fiber bundle, suggest that although our architecture is formulated to deal with situations where the fibers are topologically homogeneous, BundleNets retains sufficient expressivity to allow for more complicated relationships in the data.

6.1 Limitations

While the generative results shown above suggest that BundleNet is a powerful way to learn fibers over points, it has some drawbacks compared to other models we tested. The most glaring of these is training speed—the model (in its current form) can train slowly. This arises for two reasons: first, from our implementation of KL-divergence, which has computational complexity $\mathcal{O}(n^2)$ where n is the size of a typical neighborhood; and second from memory considerations when the data is high dimensional, since the default implementation attempts to compute loss terms using the entire neighborhood. A solution to both of these problems, we found, was to subsample the neighborhood when neighborhood size and/or dimension was too high for space and time considerations. We also found that this model was not particularly well suited to image data (partially because of dimensionality considerations). We leave it to future work to incorporate this critical modality into our fiber bundle framework.

7 Conclusion

Fibers are a useful lens through which to understand a machine learning task. However, they have been little explored in the deep learning literature so far. In this paper we showed that several promising, existing, candidate models struggled to consistently model fibers for both real and synthetic datasets. Drawing on deep ideas from topology, we introduced a new model architecture, the Bundle Network, which by design can model the fibers of a task by breaking the input space into neighborhoods and learning a function on each that decomposes input into a product of its label and all additional variation in the data. We hope this opens a door, both for applying methods from differential topology to machine learning and for further explorations into methods that can help data scientist better model and understand the fibers of their datasets.

8 Reproducibility statement

In the interest of making our results reproducible and able to be easily expanded upon, we make our codebase available to the public, including our implementations of BundleNet as well as the WGAN, CGAN, and CGAN-nbhd models we used. We also include training scripts for different models with sensible defaults as well as an evaluation script and examples. Finally, we provide the data used throughout this paper including our specific splits. This entire repository will be available on a public GitHub repository once the anonymous review period has completed.

References

- [AKRK18] Lynton Ardizzone, Jakob Kruse, Carsten Rother, and Ullrich Köthe. Analyzing inverse problems with invertible neural networks. In *International Conference on Learning Representations*, 2018.
- [AKS⁺21] Lynton Ardizzone, Jakob Kruse, Peter Steinbach, Till Bungert, Peter Sorrenson, Alexandre René, and Johnson Yue. Framework for easily invertible architectures, 2021.
- [BPM89] T. Brooks, D. Pope, and M. Marcolini. Airfoil self-noise and prediction. 1989.

- [CCA⁺09] Paulo Cortez, António Cerdeira, Fernando Almeida, Telmo Matos, and José Reis. Modeling wine preferences by data mining from physicochemical properties. *Decision support systems*, 47(4):547–553, 2009.
- [CDH⁺16] Xi Chen, Yan Duan, Rein Houthoofd, John Schulman, Ilya Sutskever, and Pieter Abbeel. Infogan: Interpretable representation learning by information maximizing generative adversarial nets. In *Proceedings of the 30th International Conference on Neural Information Processing Systems*, pages 2180–2188, 2016.
- [CLGD18] Ricky TQ Chen, Xuechen Li, Roger Grosse, and David Duvenaud. Isolating sources of disentanglement in variational autoencoders. *arXiv preprint arXiv:1802.04942*, 2018.
- [DG17] Dheeru Dua and Casey Graff. UCI machine learning repository, 2017.
- [DKB15] Laurent Dinh, David Krueger, and Yoshua Bengio. Nice: Non-linear independent components estimation. *CoRR*, abs/1410.8516, 2015.
- [DSB16] Laurent Dinh, Jascha Sohl-Dickstein, and Samy Bengio. Density estimation using real NVP. *CoRR*, abs/1605.08803, 2016.
- [Dup18] Emilien Dupont. Learning disentangled joint continuous and discrete representations. In *Proceedings of the 32nd International Conference on Neural Information Processing Systems*, pages 708–718, 2018.
- [FSV⁺19] Jean Feydy, Thibault Séjourné, François-Xavier Vialard, Shun-ichi Amari, Alain Trounev, and Gabriel Peyré. Interpolating between optimal transport and mmd using sinkhorn divergences. In *The 22nd International Conference on Artificial Intelligence and Statistics*, pages 2681–2690, 2019.
- [GBR⁺12] Arthur Gretton, Karsten M. Borgwardt, Malte J. Rasch, Bernhard Schölkopf, and Alexander Smola. A kernel two-sample test. *Journal of Machine Learning Research*, 13(25):723–773, 2012.
- [GPAM⁺14] Ian Goodfellow, Jean Pouget-Abadie, Mehdi Mirza, Bing Xu, David Warde-Farley, Sherjil Ozair, Aaron Courville, and Yoshua Bengio. Generative adversarial nets. *Advances in neural information processing systems*, 27, 2014.
- [HRU⁺17] Martin Heusel, Hubert Ramsauer, Thomas Unterthiner, Bernhard Nessler, and Sepp Hochreiter. Gans trained by a two time-scale update rule converge to a local nash equilibrium. In *Proceedings of the 31st International Conference on Neural Information Processing Systems, NIPS’17*, page 6629–6640, Red Hook, NY, USA, 2017. Curran Associates Inc.
- [Kan40] Leonid Vitalevich Kantorovich. On one effective method of solving certain classes of extremal problems. In *Dokl. Akad. Nauk. USSR*, volume 28, pages 212–215, 1940.
- [KL51] S. Kullback and R. A. Leibler. On Information and Sufficiency. *The Annals of Mathematical Statistics*, 22(1):79 – 86, 1951.
- [KM18] Hyunjik Kim and Andriy Mnih. Disentangling by factorising. In Jennifer Dy and Andreas Krause, editors, *Proceedings of the 35th International Conference on Machine Learning*, volume 80 of *Proceedings of Machine Learning Research*, pages 2649–2658. PMLR, 10–15 Jul 2018.
- [KW13] Diederik P Kingma and Max Welling. Auto-encoding variational bayes. *arXiv preprint arXiv:1312.6114*, 2013.
- [Lee10] John Lee. *Introduction to topological manifolds*, volume 202. Springer Science & Business Media, 2010.

- [LTF020] Zinan Lin, Kiran Koshy Thekumparampil, Giulia C Fanti, and Sewoong Oh. Infogan-cr: Disentangling generative adversarial networks with contrastive regularizers. In *ICML*, 2020.
- [LTH⁺17] Christian Ledig, Lucas Theis, Ferenc Huszár, Jose Caballero, Andrew Cunningham, Alejandro Acosta, Andrew Aitken, Alykhan Tejani, Johannes Totz, Zehan Wang, et al. Photo-realistic single image super-resolution using a generative adversarial network. In *Proceedings of the IEEE conference on computer vision and pattern recognition*, pages 4681–4690, 2017.
- [LTH⁺18] Hsin-Ying Lee, Hung-Yu Tseng, Jia-Bin Huang, Maneesh Singh, and Ming-Hsuan Yang. Diverse image-to-image translation via disentangled representations. In *Proceedings of the European conference on computer vision (ECCV)*, pages 35–51, 2018.
- [MLT⁺19] Qi Mao, Hsin-Ying Lee, Hung-Yu Tseng, Siwei Ma, and Ming-Hsuan Yang. Mode seeking generative adversarial networks for diverse image synthesis. In *Proceedings of the IEEE/CVF Conference on Computer Vision and Pattern Recognition*, pages 1429–1437, 2019.
- [MO14] Mehdi Mirza and Simon Osindero. Conditional generative adversarial nets. *arXiv preprint arXiv:1411.1784*, 2014.
- [Mog16] Olof Mogren. C-rnn-gan: Continuous recurrent neural networks with adversarial training. *arXiv preprint arXiv:1611.09904*, 2016.
- [RM15] Danilo Jimenez Rezende and Shakir Mohamed. Variational inference with normalizing flows. In *Proceedings of the 32nd International Conference on International Conference on Machine Learning - Volume 37, ICML’15*, page 1530–1538. JMLR.org, 2015.
- [Sei33] H. Seifert. Topologie Dreidimensionaler Gefaserner Räume. *Acta Mathematica*, 60(none):147 – 238, 1933.
- [SGZ⁺16] Tim Salimans, Ian Goodfellow, Wojciech Zaremba, Vicki Cheung, Alec Radford, and Xi Chen. Improved techniques for training gans. In *Proceedings of the 30th International Conference on Neural Information Processing Systems, NIPS’16*, page 2234–2242, Red Hook, NY, USA, 2016. Curran Associates Inc.
- [SLJ⁺15] Christian Szegedy, Wei Liu, Yangqing Jia, Pierre Sermanet, Scott Reed, Dragomir Anguelov, Dumitru Erhan, Vincent Vanhoucke, and Andrew Rabinovich. Going deeper with convolutions. In *2015 IEEE Conference on Computer Vision and Pattern Recognition (CVPR)*, pages 1–9, 2015.
- [SLY15] Kihyuk Sohn, Honglak Lee, and Xinchen Yan. Learning structured output representation using deep conditional generative models. *Advances in neural information processing systems*, 28:3483–3491, 2015.
- [SRK20] Peter Sorrenson, Carsten Rother, and Ullrich Köthe. Disentanglement by nonlinear ICA with general incompressible-flow networks (GIN). *CoRR*, abs/2001.04872, 2020.
- [Vas69] Leonid Nisonovich Vaserstein. Markov processes over denumerable products of spaces, describing large systems of automata. *Problemy Peredachi Informatsii*, 5(3):64–72, 1969.
- [Whi35] Hassler Whitney. Sphere-spaces. *Proceedings of the National Academy of Sciences*, 21(7):464–468, 1935.
- [WHT⁺18] Jiqing Wu, Zhiwu Huang, Janine Thoma, Dinesh Acharya, and Luc Van Gool. Wasserstein divergence for gans. In *Proceedings of the European Conference on Computer Vision (ECCV)*, pages 653–668, 2018.
- [WKV09] Qing Wang, Sanjeev R. Kulkarni, and Sergio Verdu. Divergence estimation for multidimensional densities via k -nearest-neighbor distances. *IEEE Transactions on Information Theory*, 55(5):2392–2405, 2009.

A Appendix

A.1 Datasets

In this section we document our method for either generating or modifying datasets used in this work.

Torus: This is a purely synthetic dataset that uses an embedding of a torus (a 2-dimensional surface/manifold) in \mathbb{R}^3 . Given two radii r and R , the torus parameterization is given by:

$$T(r, R) = \{(R + r \cos \theta) \cos \phi, (R + r \cos \theta) \sin \phi, r \sin \theta) : 0 \leq \phi, \theta < 2\pi\}.$$

Our data uses $R = 8$ and $r = 2$ and consists of 1000 points generated by uniformly sampling parameters ϕ and θ from $[0, 2\pi)$. Notice that this does not represent a uniform sampling from the surface itself since it more heavily represents the inner ring of the torus. When we evaluate, we use rejection sampling to sample uniformly from the surface. The base space Y is given by a circle of radius 4.5.

Möbius band: This is our second synthetic data and another surface in \mathbb{R}^3 . This one is given by the parameterization:

$$M(r, R) = \{(R \cos \theta, R \sin \theta, 0) + s \cdot A_\theta B_{\frac{\theta}{2}} A_\theta^{-1}(-\cos \theta, -\sin \theta, 0) : 0 \leq \theta < 2\pi, -r \leq s \leq r\}$$

where A_θ is the rotation matrix around the z -axis through the angle θ and B_θ is the rotation matrix around the x axis through the angle θ . Our data (both for training and evaluation) consists of 1000 points with $r = 2$ and $R = 8$ which are sampled uniformly over the parameters θ and s . The base space Y is a radius 4.5 circle.

The two real-world datasets, **Wine Quality** [CCA⁺09] and **Airfoil Noise** [BPM89], are described more completely on their pages in the UCI ML repository [DG17]. The Wine Quality dataset is provided as two files (for red and white wine) with the intention of predicting quality from 11 measured quantities. We combine these two sets into one so that we have 11 inputs and two (both categorical) outputs: color and quality. The Airfoil Noise dataset has 5 input parameters and one output parameter (scaled sound pressure level), which we left unaltered. As a pre-processing step we normalized all parameters in each datasets to span the range 0 to 10 by applying $x \mapsto \frac{10}{M}(x - m)$ where m and M are the minimum and maximum values of each parameter. We made an 80/20% train/test split for each.

A.2 Loss functions and evaluation metrics

There has been much work in the world of GANs to establish metrics that can quantify the quality of a generative model. This includes the widely-used Inception Score [SGZ⁺16] and Fréchet Inception Distance [HRU⁺17]. Many of these metrics, however, rely on the assumption that the data has the structure of an image. For instance, in both the methods mentioned above one computes these metrics by using a pretrained Inception v.3 model [SLJ⁺15] to extract latent features from generated images. One then uses methods from statistics/optimal transport like the Wasserstein distance or Kullback-Leibler divergence to evaluate similarity under the assumption that data in these latent spaces follow Gaussian distributions.

Since the data we are using are not images, and since the assumption that our data follows some Gaussian distribution is catastrophically restrictive, we choose some standard two-sample tests to quantitatively compare the performance of different models. One could make the argument that with the blessing of low-dimensionality we are able to more directly access the metrics that are only being approximated in methods such as those for images that rely on a pretrained classifier model.

Mean squared minimum distance: The simplest of our metrics, the mean squared minimum distance (MSMD) takes two samples S_1 and S_2 and computes

$$\text{MSMD}(S_1, S_2) = \frac{1}{|S_1|} \sum_{x_1 \in S_1} \min_{x_2 \in S_2} \|x_1 - x_2\|^2.$$

This naïve approach is not as robust to different distributions as the methods that follow, but in the case that S_2 is a collection of points uniformly distributed on some known space (e.g. a circle in space corresponding

to the true fiber over a point), this number is more readily interpretable as an approximate measure of how “realistic” the points in S_1 are, given the region containing S_2 .

Kullback-Leibler divergence: The KL-divergence, or *relative entropy* was a test introduced by [KL51] to apply an information-theoretic approach to the problem of detecting *divergence* of two samples by attempting to quantify the amount of signal (or information) that one could use to distinguish between the two. For instance, given two distributions P and Q on \mathbb{R} with densities p and q , this quantity is given by

$$D_{\text{KL}}(P||Q) = \int_{-\infty}^{\infty} p(x) \log \left(\frac{p(x)}{q(x)} \right) dx.$$

A problem that needs to be solved to apply the KL-divergence to our samples is to fix a method of density estimation. A suggestion by [WKV09] is to (for some integer hyperparameter k) approximate the density using the k^{th} nearest neighbor of a point in each population. This approximation is fast and easily made to be differentiable and for this reason we use it both in our loss function and as an evaluation metric.

Note that the KL-divergence is not an honest metric and in particular is *not symmetric*. The forward divergence (KL-fwd) is $D_{\text{KL}}(P||Q)$ where P is the true/target distribution and the backward divergence (KL-bwd) is $D_{\text{KL}}(Q||P)$. One way of thinking of this difference is that $D_{\text{KL}}(P||Q)$ measures how well Q covers P and vice versa. We include both separately in our results to give a holistic view of the performance.

Wasserstein metric: The Wasserstein family of metrics discovered in many works including [Kan40] and [Vas69] are based on the idea of measuring the amount of work that would need to be done to transport the (probability) mass of one distribution to another. Let $(\mathcal{X}, d_{\mathcal{X}})$ be a metric space and μ, ν probability measures on \mathcal{X} . For any $p > 0$, one defines the p -Wasserstein distance between these two distributions to be

$$W_p(\mu, \nu) = \left(\inf_{\gamma \in \Gamma(\mu, \nu)} \int_{(x, y) \in \mathcal{X} \times \mathcal{X}} d_{\mathcal{X}}(x, y)^p d\gamma(x, y) \right)^{1/p}$$

where $\Gamma(\mu, \nu)$ denotes the space of probability measures on $\mathcal{X} \times \mathcal{X}$ with margins μ and ν . To implement this, we piggyback off the work of [FSV⁺19], who provide a wonderful library `geomloss` of differentiable PyTorch implementations of many two-sample distances.

Maximum mean discrepancy: First introduced in [GBR⁺12], the maximum mean discrepancy (MMD) between two samples is computed by appealing to a dual problem: consider a collection of functions \mathcal{F} from our probability space \mathcal{X} to \mathbb{R} . Then the MMD can be thought of as an expression of how “different” two distributions can look under different choices of $f \in \mathcal{F}$. More concretely,

$$\text{MMD}(\mathcal{F}; P, Q) = \sup_{f \in \mathcal{F}} (\mathbb{E}_{x \sim P}[f(x)] - \mathbb{E}_{y \sim Q}[f(y)]).$$

An implementation of MMD can be found in `geomloss` [FSV⁺19] using a single Gaussian kernel.

A.3 Hyperparameters

Below we document our choices of hyperparameters for our models. ‘Neural net depth/width’ describes the structure of the MLP that is used in each model (although in subtly different ways). For our model, these parameters describe the neural nets that predict the weights and biases for our RNVP blocks. For the GAN models, these parameters control the size/shape of the generator and discriminator. ‘Num. neighborhoods’ is only applicable in models that compute neighborhoods to condition upon (i.e. BundleNet and CGAN-nbhd). ‘Num. invertible blocks’ gives the number of RNVP blocks and only applies to our architecture. ‘Num. circular priors’ again only applies to our model and implicitly defines the number of Gaussian priors we use as well. The formula is $B + 2C + G = D$ where C is the number of circles, B the dimension of the output data, G the number of Gaussian priors, and D the total/latent dimension.

Mathematically, the combination of one-dimensional priors represents a (tensor) product of distributions, but in practice this has a simple form. For each neighborhood, data from the bundle is pushed forward through the encoder to get sample statistics including the coordinate-wise means and standard deviations as well as the mean and standard deviation of the magnitudes for each circular prior. These sample statistics are used to pick a radius for each circular prior and to reparameterize a standard normal distribution for the Gaussian priors. Every circle is encoded in two parameters as a circle with the radius determined above and every Gaussian (again, formed using sample statistics) occupies a single parameter. The values are sampled independently from their respective distributions and then concatenated into a vector in latent space representing a sample from \mathcal{D}_Z .

Table 5: Hyperparameter choices used in all models trained and evaluated during the course of this work (unless otherwise noted in the main text). If multiple values are given, the format is (torus, Möbius band, wine, airfoil).

MODEL HYPERPARAMETERS				
	BundleNet (ours)	WGAN	CGAN	CGAN-nbhd
Initial learning rate	10^{-4}	10^{-4}	10^{-4}	10^{-4}
Latent dimension	(8, 8, 8, 12)	10	10	10
Neural net depth.	5	5	5	5
Neural net width.	512	128-1024	128-1024	128-1024
Num. neighborhoods	(25, 25, 13, 25)	N/A	N/A	(25, 25, 13, 25)
Num. invertible blocks	5	N/A	N/A	N/A
Num. circular priors	3	N/A	N/A	N/A

A.4 Generating synthetic data

We include some visualizations of the torus and Möbius band (both global and fiberwise) reconstructed by BundleNet. Notice not only the clarity of the global picture, but the fact that our model is able to reconstruct reasonable approximations of the fibers in each map: a twisting line segment in the case of the Möbius band and a circle in the case of the torus. Each global point cloud consists of 20000 points and each individual generated fiber consists of 100 points.

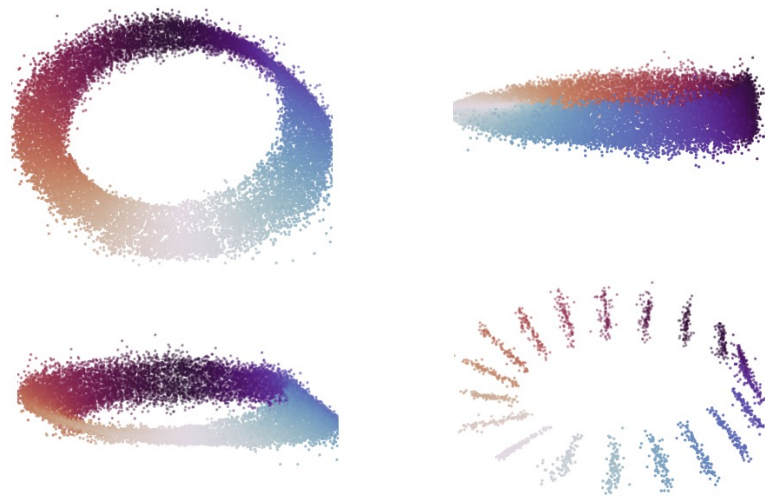


Figure 5: BundleNet’s ability to generate points on a Möbius band.

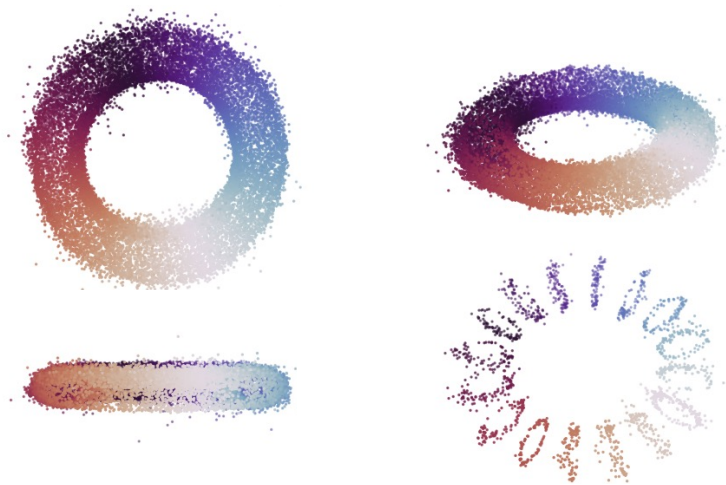


Figure 6: BundleNet’s ability to generate points on a Torus.

A.5 Full results

Below we recreate the full table of results with all metrics tested.

Table 6: Generative performance metrics (global). Each metric is applied to a trained model as detailed in section 5.1 with 95% confidence intervals determined by bootstrapping. Conditioning, when built into the model, is used to generate points over (uniformly sampled) base points to construct the point cloud.

TORUS				
	BundleNet (ours)	WGAN	CGAN	CGAN-nbhd
MSMD	0.118 ± 0.003	4.863 ± 0.043	36.10 ± 0.165	59.33 ± 0.280
MMD ($\times 10^{-3}$)	0.691 ± 0.025	3.869 ± 0.030	34.92 ± 0.319	402.5 ± 1.000
KL-Fwd	1.431 ± 0.035	6.308 ± 0.022	10.61 ± 0.036	11.42 ± 0.022
KL-Bwd	0.396 ± 0.030	5.389 ± 0.029	11.96 ± 0.022	17.45 ± 0.023
\mathcal{W}_1	0.706 ± 0.018	2.192 ± 0.010	7.113 ± 0.024	7.908 ± 0.016
\mathcal{W}_2	1.075 ± 0.071	3.404 ± 0.062	25.76 ± 0.149	32.35 ± 0.127

MÖBIUS BAND				
	BundleNet (ours)	WGAN	CGAN	CGAN-nbhd
MSMD	0.029 ± 0.001	3.187 ± 0.026	1.167 ± 0.016	53.22 ± 0.230
MMD ($\times 10^{-3}$)	0.509 ± 0.026	5.875 ± 0.038	5.909 ± 0.031	373.8 ± 1.021
KL-Fwd	1.031 ± 0.017	7.601 ± 0.040	5.936 ± 0.023	12.98 ± 0.028
KL-Bwd	0.002 ± 0.018	7.174 ± 0.044	5.832 ± 0.040	17.05 ± 0.013
\mathcal{W}_1	0.264 ± 0.004	2.048 ± 0.013	1.844 ± 0.015	7.764 ± 0.008
\mathcal{W}_2	0.060 ± 0.009	2.829 ± 0.053	2.384 ± 0.051	30.61 ± 0.064

WINE QUALITY				
	BundleNet (ours)	WGAN	CGAN	CGAN-nbhd
MSMD	1.581 ± 0.023	68.26 ± 1.436	6.630 ± 0.084	7.443 ± 0.191
MMD ($\times 10^{-3}$)	0.820 ± 0.014	95.59 ± 1.488	10.67 ± 0.123	9.683 ± 0.115
KL-Fwd	3.158 ± 0.062	24.74 ± 0.142	9.966 ± 0.114	11.07 ± 0.103
KL-Bwd	2.902 ± 0.120	115.7 ± 0.336	19.28 ± 0.132	19.30 ± 0.118
\mathcal{W}_1	1.733 ± 0.011	99.22 ± 0.392	4.054 ± 0.014	4.405 ± 0.013
\mathcal{W}_2	2.155 ± 0.036	6271. ± 40.40	8.950 ± 0.066	10.38 ± 0.066

AIRFOIL NOISE				
	BundleNet (ours)	WGAN	CGAN	CGAN-nbhd
MSMD	0.512 ± 0.022	24.54 ± 0.356	3.474 ± 0.057	12.28 ± 0.157
MMD ($\times 10^{-3}$)	1.840 ± 0.013	38.86 ± 0.480	4.222 ± 0.044	9.384 ± 0.182
KL-Fwd	5.810 ± 0.089	14.87 ± 0.059	9.131 ± 0.064	12.66 ± 0.077
KL-Bwd	2.430 ± 0.018	15.96 ± 0.058	6.716 ± 0.036	8.867 ± 0.040
\mathcal{W}_1	1.448 ± 0.022	4.741 ± 0.034	2.508 ± 0.025	4.279 ± 0.019
\mathcal{W}_2	1.888 ± 0.123	13.95 ± 0.198	4.964 ± 0.120	12.20 ± 0.100

Table 7: Generative performance metrics (fiberwise). Results were obtained by randomly sampling 5 base points and generating points in the fiber over each. Each metric is applied to the generated points and points sampled from the true distribution and averaged. Intervals represent 95% CIs over 10 repeated experiments. WGAN is excluded since it has no built-in way to condition on the base point.

TORUS			
	BundleNet (ours)	CGAN	CGAN-nbhd
MSMD	0.055 ± 0.004	29.57 ± 1.136	56.66 ± 0.563
MMD ($\times 10^{-3}$)	20.89 ± 0.935	83.77 ± 0.001	321.8 ± 5.072
KL-Fwd	18.61 ± 0.217	45.14 ± 0.330	48.18 ± 0.136
KL-Bwd	3.186 ± 0.134	25.09 ± 0.153	34.67 ± 0.154
\mathcal{W}_1	0.743 ± 0.026	7.979 ± 0.022	8.044 ± 0.021
\mathcal{W}_2	0.605 ± 0.035	32.46 ± 0.165	33.38 ± 0.164

MÖBIUS BAND			
	BundleNet (ours)	CGAN	CGAN-nbhd
MSMD	0.009 ± 0.001	0.810 ± 0.125	52.96 ± 0.351
MMD ($\times 10^{-3}$)	20.82 ± 2.724	144.0 ± 0.482	397.9 ± 6.246
KL-Fwd	7.646 ± 0.125	14.31 ± 0.146	21.43 ± 0.045
KL-Bwd	1.856 ± 0.106	8.566 ± 0.068	13.39 ± 0.031
\mathcal{W}_1	0.279 ± 0.011	9.860 ± 0.038	7.958 ± 0.022
\mathcal{W}_2	0.071 ± 0.008	58.47 ± 0.364	32.18 ± 0.209

WINE QUALITY			
	BundleNet (ours)	CGAN	CGAN-nbhd
MSMD	3.234 ± 0.883	10.70 ± 1.703	16.82 ± 3.452
MMD ($\times 10^{-3}$)	21.84 ± 13.08	48.37 ± 40.40	61.70 ± 22.82
KL-Fwd	-0.091 ± 1.186	5.942 ± 1.303	8.452 ± 1.254
KL-Bwd	0.856 ± 0.474	10.56 ± 1.468	11.67 ± 1.253
\mathcal{W}_1	1.917 ± 0.172	3.666 ± 0.233	4.408 ± 0.457
\mathcal{W}_2	2.407 ± 0.763	7.941 ± 0.951	11.23 ± 2.235

AIRFOIL NOISE			
	BundleNet (ours)	CGAN	CGAN-nbhd
MSMD	1.920 ± 0.157	2.793 ± 0.367	5.155 ± 0.352
MMD ($\times 10^{-3}$)	35.872 ± 1.253	37.37 ± 0.935	39.504 ± 0.975
KL-Fwd	-2.694 ± 0.430	-1.259 ± 0.543	0.423 ± 0.414
KL-Bwd	3.250 ± 0.085	4.908 ± 0.175	6.943 ± 0.142
\mathcal{W}_1	3.124 ± 0.089	3.563 ± 0.158	3.794 ± 0.128
\mathcal{W}_2	6.744 ± 0.459	8.054 ± 0.711	8.834 ± 0.654